# Control Systems - ELEN90055

## *Workshop 4*

George Juliff – 624946

Kweku Acquah – 741573

Thomas Miles – 626263

2018

Semester 1

# 1   Introduction

This report proposes a control system which can maintain an inverted pendulum upright under the presence of external disturbances and sensor noise. The system used a phase-lead feedback controller to achieve robust behaviour, insensitive to modelling errors and a range of operating conditions.

Controller programming, analysis, and interfacing with the *LEGO MINDSTORMS EV3* was completed using Simulink and Matlab, which provide a vast library of tools for system analysis and hardware control.

Using mathematical models for the robot's electrical and physical dynamics, the controller was designed to meet a set of operating requirements discussed in detail in section 3.

# 2   System Modelling

## 2.1   Building the Inverted Pendulum Model

The mathematical models for the system were derived from basic physics principles; then using kinematics the physical properties of the system were then found via experiment. By developing this set of ODEs, a transfer function relating angular displacement (from a gyroscope sensor attached to the pendulum) to a motor voltage command.

## 2.2   Mathematical Model of the Inverted Pendulum

Figure 1: Inverted Pendulum and DC Motor Systems
Credit: M. Cantoni, The University of Melbourne, ELEN90055 Problem Set 1.

Figure 1 demonstrates a simplified inverted pendulum and DC motor circuit where:

- $J = (J_m + ml^2)$: moment of inertia of the motor and load relative to the motor shaft (kg.m2)

- $b$: viscous damping of shaft ($N.s/m$)

- $\theta$: angular displacement of the motor shaft (rad)

Figure 2: Free Pendulum Model

Using the Newton-Euler equation for the angular acceleration of the pendulum about the motor shaft:

$$M = J\ddot{\theta}$$
$$mgl\sin(\theta) - T_{damping} = (J_m + ml^2)\ddot{\theta}$$
$$mgl\sin(\theta) - b\dot{\theta} = (J_m + ml^2)\ddot{\theta}$$
$$mgl\sin(\theta) = (J_m + ml^2)\ddot{\theta} + b\dot{\theta}$$

Assuming small values for theta:

$$\Rightarrow mgl\sin(\theta) + b\dot{\theta} = (ml^2)\ddot{\theta} \qquad (1)$$

To determine the physical properties of the system, the pendulum was allowed to swing un-actuated and it's motion was measured using the gyro. Subsequently, equation (1) can be solved numerically, systematically varying physical parameters to find a model that is accurate to the experimental data obtained.

## 2.3   Experimental Data vs Calculated Data

Experimental data obtained from displacing the pendulum as shown in Figure 3 where the initial conditions were $\dot{\theta}(0) = 0$ and $\theta(0) = \frac{\pi}{2}$ produced the figure below:

Figure 3: Free Pendulum Results

By trial-and-error, the following parameter values for $m$, $l$, and $b$ were chosen to obtain a suitable ODE solution set:

$$m = 0.20 \quad \text{Kg}$$
$$l = 0.11 \quad \text{m}$$
$$b = 0.004 \quad \text{N.s/m}$$

where $g = 9.81$ m/s$^2$. These values yield the model shown in Figure 4 Figure 4 clearly shows that the pa-

Figure 4: Matching Model to Experimental Results

rameter values selected do not accurately represent the physical system. There is a clear error between the

data obtained from the gyro sensor and the data obtained from solving the ODE. However, because the form of calculated model is like the experimental data, we can be confident that developing a controller which meets the provided specifications based on this model will produce a control action suitable for controlling and responding to the dynamics of the physical system. Using the parameter values obtained we can now consider the actuated inverted pendulum system. A relevant subset of the stalled and no-load characteristics of the motor and a small-signal linearized approximation of are shown below:

$$ml^2\ddot{\theta} = \tau - b\dot{\theta} + mgl\theta$$

where

$$\tau = \frac{Kt}{R}(v - K_b\dot{\theta})\text{and}$$
$$\frac{K_t}{R} = 1.66 \times 10^-2\frac{N.m}{V}$$
$$K_b = 0.297\frac{V \cdot \text{sec}}{\text{rad}}$$

Taking the Laplace Transform of the small-signal linear approximation and accounting for the "percentage full power" units of the motor command (percentage of 9 V) and gyro sensor and motor encoder angle measurement units (in degrees) yields the following transfer function between the motor command and pendulum angle in degrees:

$$G(s) = \frac{\Theta_{deg}(s)}{V_\%(s)} \qquad \frac{\text{degrees}}{\%\text{ full power}}$$
$$\Rightarrow G(s) = \frac{9}{100} \cdot \frac{180}{\pi} \cdot \frac{\frac{K_t}{R}}{(s^2 \times ml^2 + s \times (b + \frac{K_tK_b}{R}) - mgl)}$$

Substituting the system parameters yields the model we used to develop our controller:

$$G(s) = 0.086090 \cdot 00242s^2 + 0.008959s - 0.2158$$

# 3 Controller Design

## 3.1 Performance Requirements

The controller should:

1. Reject impulsive and step disturbances, imparted by manual displacement of the pendulum and turning the robot caused by the drive wheels respectively.

2. Be internally stable.

3. Have a phase margin of 40° or more.

4. Have a complimentary sensitivity function bandwidth of less than 50 rad/sec.

## 3.2 Controller Implementation

The controller used to achieve these requirements was a phase lead controller, of the form:

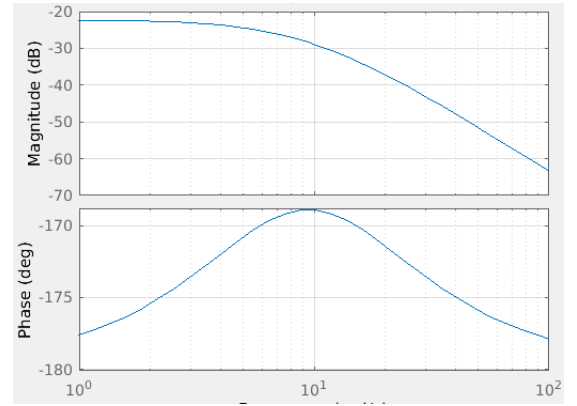$$C(s) = 100 \cdot \frac{(0.1s + 1)}{0.001s + 1}$$



Figure 5: Bode Plot of Plant Model

### Model Considerations to Meet Requirements

- *Meeting the phase requirement.* Observing the phase part of Figure 5, it can be seen that to achieve the required phase margin the controller needs to add phase at crossover.

- *Internal stability.* Figure 6 shows the root locus plot of the plant transfer function detailed in section 2. Because the model contains an unstable pole, sufficient gain to stabilise it must be used. Since the relative degree of the model is two, during controller design care was taken to avoid excessive gain values which develop undesirable oscillations in the system.
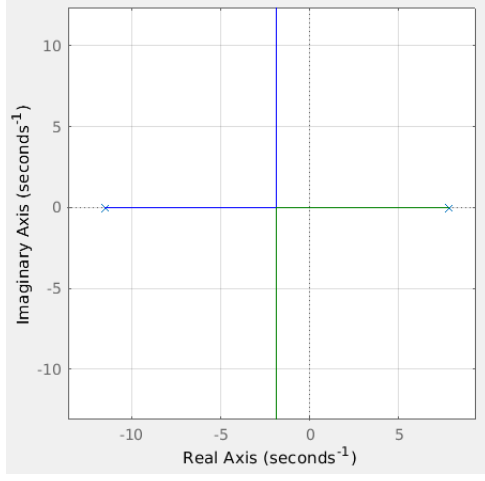
Figure 6: Root Locus of Plant Model

**Loop Shaping**

The zero used in the controller was chosen to be placed between the poles in the plant model, this serves to completely stabilise the unstable pole in the plant for sufficiently high K.
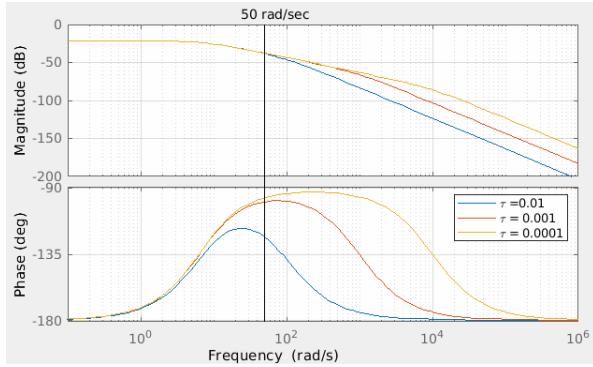


Figure 7: Effect of Pole Placement on Complimentary Sensitivity Function

Varying the position of the pole in the nominal controller transfer function $\frac{0.1s+1}{\tau s+1}$, Figure 7 shows that phase increases when $\tau$ is decreased, thus as the pole moves away from the origin. To meet the design requirements, the crossover frequency of the complimentary sensitivity function $T_0$ to be less than 50 rad/sec. Furthermore, to track desired inputs well, the magnitude of the complimentary sensitivity function at low frequencies should be close to 1 dB. Figure 7 demonstrates the phase margin at maximum crossover frequency (50 rad/sec) for $\tau = 0.01$ is substantially lower when compared to the smaller values of $\tau$. $\tau = 0.001$ and $\tau = 0.0001$ have similar phase margins at 50 rad/sec crossover, with even lower discrepancy at lower

crossover frequencies. Therefore, since $\tau = 0.001$ drops off sooner (making it less susceptible to sensor noise), this value was used in the controller.
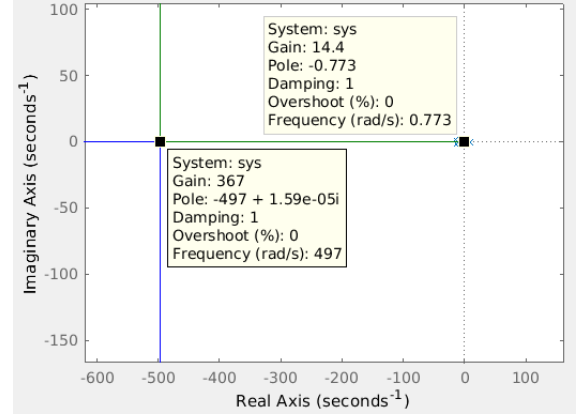


Figure 8: Root Locus of Open Loop System

Finally, based on Figure 8, the system is internally stable and non-oscillatory for $15 < K < 360$. In order to meet the sensitivity and physical behaviour requirements, K = 100 was chosen, the resulting bode plot for sensitivity can be seen in Figure 9.
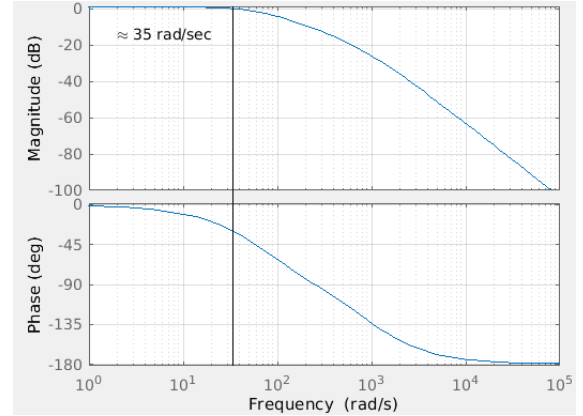


Figure 9: Bode Diagram – Complimentary Sensitivity Function, $T_0$

The crossover frequency of the sensitivity function is at approximately 30 rad/sec, which meets the sensitivity bandwidth requirement of 50hz. Furthermore, the magnitude of the sensitivity function for $\omega < 30$ rad/sec is approximately 1. This is desirable for physical performance, because overly high or low sensitivity to perturbations we which to respond to (in the lower range of frequencies) would result in over/undershooting.

**Time Domain Response** The final step in controller design prior to implementation and testing was

simulating impulse and step responses of the closed loop system. Figures ?? and ?? show the simulated responses; the behaviour is as anticipated based on prior analysis, showing no oscillation as designed.

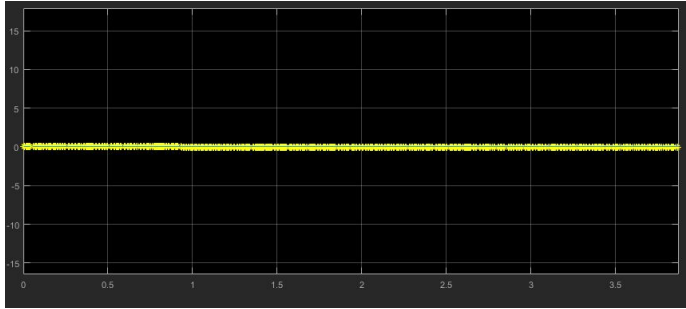# 4 Implementation and testing

## 4.1 Presentation of performance



Figure 10: Stable system without disturbance

From figure 10 it can be seen that under optimal conditions the system is perfectly stable. However, as it is possible to balance the arm in this position without the motor being driven this is not a difficult state to maintain. In figure 11 the state the arm returns to when removed from this base state is shown. While
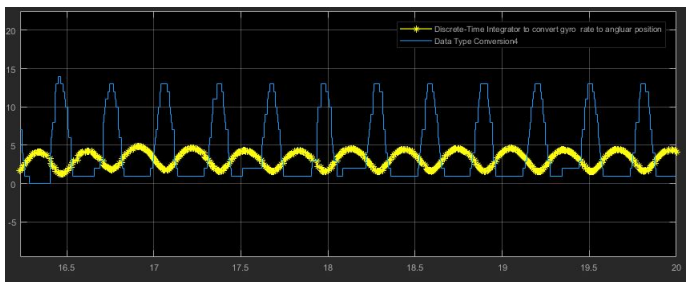


Figure 11: Return state after disturbance

the oscillation was not expected the arm is able to maintain this state indefinitely and can therefore be considered to have remained upright.

## 4.2 Assessment of design criteria

### 4.2.1 Regulation and Disturbance Rejection

Figure 12 demonstrates the systems ability to recover from an impulse disturbance. As previously mentioned it does not recover from the oscillation, although it is
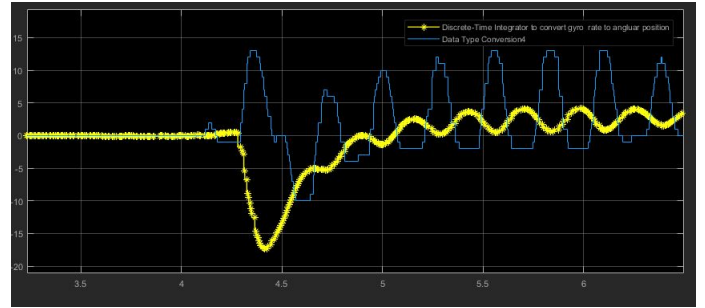


Figure 12: Impulse response

able to maintain the upright position this criterion was considered fulfilled.
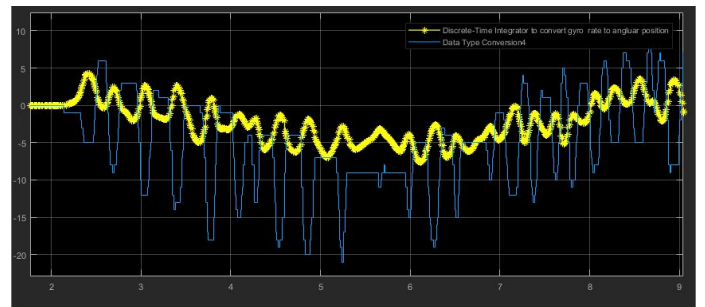


Figure 13: Steering resposnce

For the case of the system in steering mode in figure 13 the result is not so clear. While the high frequency oscillation did not present a problem there also a much lower frequency oscillation that, when compared with the steering angle in figure 14, can be seen to be related.
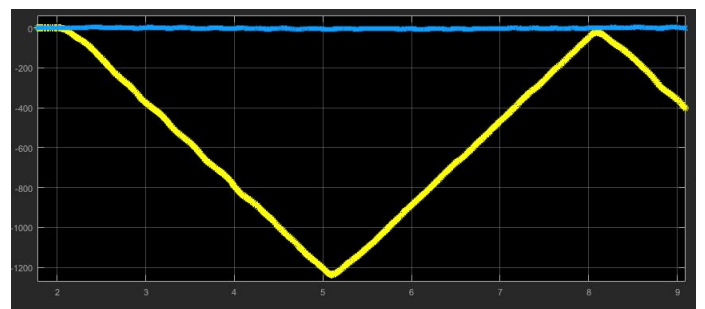


Figure 14: Steering wheel angle

While it may appear that were the turning to continue the system may fail, it can be seen this is not the case in figure 15. Ignoring the high frequency noise, a lower frequency oscillation can be seen opposing the movement of the arm. From this it can be inferred that were the steering to continue then the system would

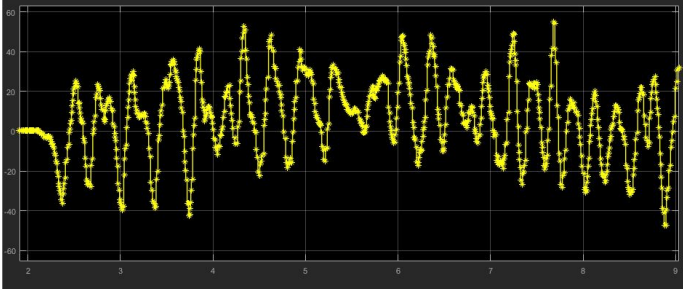remain an equilibrium where the centripetal force is balanced by the motor.



Figure 15: Motor Driving Voltage



Figure 16: Simulated impulse response

### 4.2.2 Phase Margin

Unfortunately, the phase margin could not be shown to be 40°. Adding a delay in the system corresponding to 40° at the critical frequency was the method used to test this, however, this resulted in the motor voltage repeatedly saturating and very erratic behaviour. This was due to the fact the maximum force that could be delivered by the motor was not taken into account during the design stage, and as such some boundary cases that may have appeared stable are not reliably so in practice.

### 4.2.3 Bandwidth

The bandwidth requirement could also not be shown to be fulfilled, however, this was due to an inability to test it rather than because it necessarily wasnt. The method of testing this would have been to introduce an 50rad/s signal and observe that its magnitude was reduced by more than $\sqrt{2}$. The issue was that the background oscillation of the system either overwhelmed the response for low disturbance magnitudes, or that the motors force limitation would cause the entire system to fail at high magnitudes. As such this criterium could not be verified one way or the other.

### 4.3 Comparison against simulated system

Figure 16 shows the predicted impulse response of the system, and when compared to figure 12 several differences can be observed. Most immediately the oscillation present in the system is absent from the model.
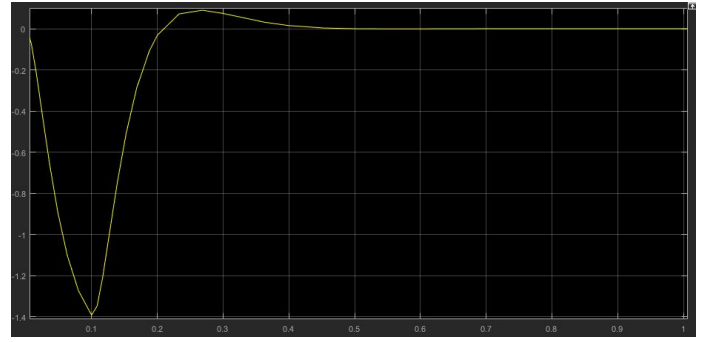
In addition, it is clear the system is significantly more damped than the model as on returning to steady state the system displays no overshoot and is significantly slower to do so.

There are several reasons this might be the case. The damping effect is likely primarily due to the unmodeled limitations of the motor rather than any real damping. The motor is unable to apply the full expected force that is applied in the model and this results in a damping like effect when the controller voltage saturates.

The oscillation on the other hand is likely caused by the assumptions made during the modelling. Namely the assumption that the motor is completely fixed. In reality it could be seen that the motor was able to shift in the robot, and in addition the entire robot would shift with the pendulum. This added motion was not accounted for and likely the primary reason for the oscillation although there were doubtless other contributing factors.

## 5 Conclusion

While we were unable to demonstrate that all of the criteria discussed in 3 were met, we were able to demonstrate through experiment and calculation that the system is robust and stable. Furthermore we analysed and discussed the shortcomings of our control system, and why the realised system behaves differently to the modelled one.

Improvements could certainly be made to the model in order to better fulfil the design criteria. However better modelling the system would exponentially in-

crease the mathematical complexity of the problem, and as such further experimentation my be the best way to find an improved model.